Dear Editors and Anonymous Reviewers:

We greatly appreciate reviewer's insightful and helpful comments regarding our manuscript. The manuscript has been revised based on reviewer's comments. Following the reviewers' suggestions, the revised manuscript provides a more detailed description based on the theories of Reichl and Deike (2020) as well as the $dpCO_2$-driven negative feedback mechanism and carbonate–pH system adjustment associated with ocean buffering effects, consistent with the findings of Rustogi et al. (2025).

In addition, we moved the descriptions of the model framework, experiments, and POP2–waves coupling methodology to the beginning of Section 2, while the introduction of the model validation data was moved to the end of Section 2. This restructuring provides a more direct and coherent presentation of the model framework. The reworded results are presented alongside the relevant figures and discussed within a broader scientific context. Below are the point-by-point responses to the comments and concerns raised by Anonymous Referee #1 (pp. 1–14) and Anonymous Referee #2 (pp. 14–30).

Sincerely,
Yung-Yao Lan, Huang-Hsiung Hsu, Wei-Liang Lee and Simon Chou

Anonymous Referee #1 (pp.1–14)

The reviewer comments are formatted in italics and the authors response to the comments are formatted in bold.

Notation *RC1.P#* represents Reviewers Comment. Paragraph Number

Specific comments:

RC1.1 Consider using the revised version of Kw from Wanninkhof (2014) instead of Wanninkhof (1992).

Response:

Thank you for pointing out the mistake. In the B-CTL control experiment, the coefficient (*k*) for gas transfer velocity in Equation (2) follows Wanninkhof (1992), where k = 0.31. I mistakenly entered 0.251, which may have led to confusion with Wanninkhof (2014); this has now been corrected in the revised manuscript. For further details, please refer to the original CESM1 POP2 code (ecosys_mod.F90), specifically the annotation of the variable *xkw_coeff* (! a = 0.31 cm/hr s^2/m^2 in (s/cm)) and Table RC1.1.

Table RC1.1 The coefficient (*k*) used to parameterize gas transfer velocity (K_w) differs between Wanninkhof (1992) and Wanninkhof (2014).

	Wanninkhof (1992)	Wanninkhof (2014)
the coefficient (*k*) of gas transfer velocity (K_w) $K_w = k <U_{10}^2> (Sc/660)^{-0.5}$	0.31	0.251
optimal method	applicable to deduce K_w	The optimal coefficient was

	at steady winds	**obtained using an inverse modeling approach with CCMP[1] winds and the Modular Ocean Model General Circulation Model (MOM3 GCM).**

Note:[1]CCMP: The Cross-Calibrated Multi-Platform (CCMP) are produced by Remote Sensing Systems (RSS) with support from a NASA Ocean Vector Winds Science Team grant.

RC1.2 L78-L87: the text on direct flux observations requires revisions. When referring to 'direct observations' in this context, it is usually understood 'direct flux measurements'. However, here the authors first refer to pCO_2 observations and then to direct fluxes using eddy covariance. Please revise the text to increase clarity. Also note that direct fluxes using eddy covariance can be made with both open- and close-path analyzer, which is not mentioned in the text. Furthermore, data assimilation is mentioned here, where it seems rather isolated. Please provide the necessary information to present a sound context for the reader.

Response:

Thank you for your suggestion. The L78-L87 lacked a complete and coherent description. The revised version is as follows:

Direct flux measurements in marine environments using the eddy covariance method can be conducted with both open- and closed-path analyzers. A closed-path infrared gas analyzer (e.g., LI-7000, LI-COR) operates with an enclosed measurement chamber (Sutton et al., 2014, 2021; Bakker et al., 2016; Sabine et al., 2020; Akhand et al., 2021; Wu and Qi, 2023), whereas open-path analyzers (e.g., LI-7500, LI-COR) measure infrared absorption directly in ambient air (Edson et al., 2011; Tokoro et al., 2014; Bell et al., 2017; Dong et al., 2021; Van Dam et al., 2021). Both types are affected by H_2O cross-sensitivity, but each has its own advantages and limitations (Honkanen et al., 2018).

RC1.3. Section 2.1 should not be called 'observational data', this is misleading as the NOAA CarbonTracker is not only based on observations, but largely on model predictions and numerical techniques to estimate the fluxes.

Response:

We have changed the title of Section 2.1 from "Observational Data" to "Model Validation Data" and revised several sentences in this section to provide a better introduction to CarbonTracker and to avoid using the phrase "sources and sinks of CO_2 flux."

RC1.4. As mentioned above, the methodology section requires substantial improvements. This is particularly important given that the manuscript is submitted to a model development journal. Therefore, strong emphasis should be made in presenting the relevant aspects of such model development. In this case, details about the wave module and its implementation in POP2 is of particular relevance. However, other aspects are also lacking. For example, details about the CarbonTracker, details of each of the models and model components, information about input data, forcing, etc. The authors mention pCO2, pH and the 'POP2 (bio)geochemistry response' in the methodology section, but there is no information about the biogeochemical module, and this is not included in the architecture diagram in figure 1 either. This is all essential for the reproducibility of the results.

Response:

Thank you for your suggestion. We have substantially revised the methodology section of the manuscript, including (1) the development of the CESM1–POP2–waves model and its component modules (Sections 2.2 and 2.3), (2) a more detailed description of CarbonTracker (Section 2.1), (3) additional information on POP2–waves input data and atmospheric forcing (Sections 2.2 and 2.3), and (4) an expanded description of the Marine Biogeochemistry (MARBL) module in Section 2.2 and Fig. 1, highlighting that all components influence the air–sea CO_2 flux. Please refer to the revised manuscript for details of these changes.

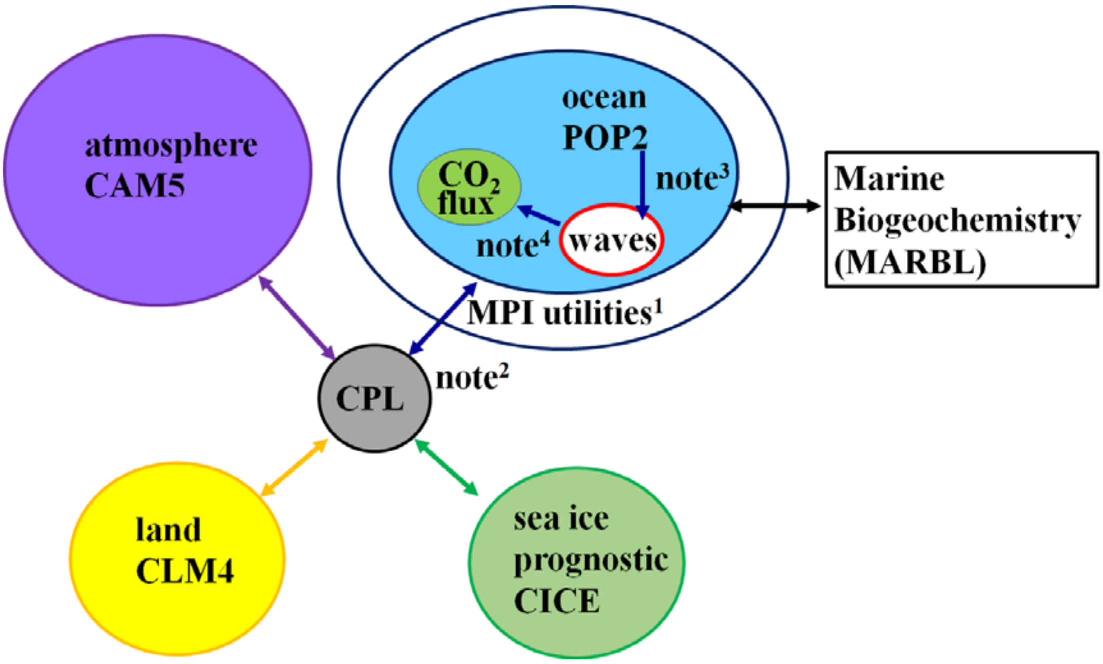

Figure 1. Architecture diagram for POP2–waves experiment in CESM1.2.2 framework, all components adhere to the CESM 1.2.2 framework, except for

certain parts of the ocean component. The model components including components for the atmosphere [Community Atmosphere Model version 5 (CAM5)], land [Community Land Model version 4 (CLM4)], ocean [Parallel Ocean Program, version 2 (POP2)], along with its associated modules—the waves module (waves) and the Marine Biogeochemistry (MARBL) module—sea ice [prognostic Los Alamos Sea Ice Model (CICE)], and the coupler (CPL).

Note:
[1]The wave-module variables are communicated between neighboring blocks via MPI, including zonal and meridional 10-m winds, wave radiation stress, subsurface momentum, and wave radiation and energy densities.
[2] To transfer variables such as zonal and meridional 10-m winds and friction velocity (including sea surface and ice fraction) from the CPL to POP2.
[3] The wave module receives variables from POP2, including the interpolation of depth-varying currents from z-coordinates (60 levels) to the wave module's vertical sigma coordinates (21 levels), along with ocean grid information in the x, y, and z directions.
[4] The wave module outputs significant wave height and friction velocity from the CPL for calculating the bubble-mediated gas transfer velocity in Eq. (3).

RC1.5. Following on my previous comment, Section 2.3 should include much more than 10 lines on the coupling of POP2-waves. The information here should be enough for a reader to be able to reproduce the results!

Response:

In Section 2.3, we have provided more than 20 lines describing the coupling of POP2-waves. The revised manuscript explains how the wave module is integrated into POP2, including vertical coordinate transformation, required external input files, and its parallel computing implementation within the CESM1.2.2 framework, as well as the improvements shown in Fig. 1.

RC1.6. There is a notation issue that can cause confusion. The authors refer to the gas transfer velocity as Kw, often mentioning Kw from W92, i.e. eq (2). However, in eq. (3) Kw is not only the wind-based component of the parametrization, but the total gas transfer velocity (i.e. including waves), and KwNB refers to wind-based component from W92, not Kw anymore. Please, use a consistent notation.

Response:

In Eqs. (2–3), K_w in both equations represents the total gas transfer velocity; in Eq. (2), it follows W92, whereas in Eq. (3), it is based on Deike and Melville (2018). In Eq. (3), K_w consists of two components: the non-bubble term ($K_{w,NB}$) and the bubble term ($k_{w,B}$). The $K_{w,NB}$ is based on the friction velocity, u_* (m s^{-1}) as shown in the shaded area of Fig. 7(d), and therefore differs from W92, which is based on the squared 10-m wind speed as shown in the shaded area of Fig. 7(c) or the Fig. RC1.6.1.

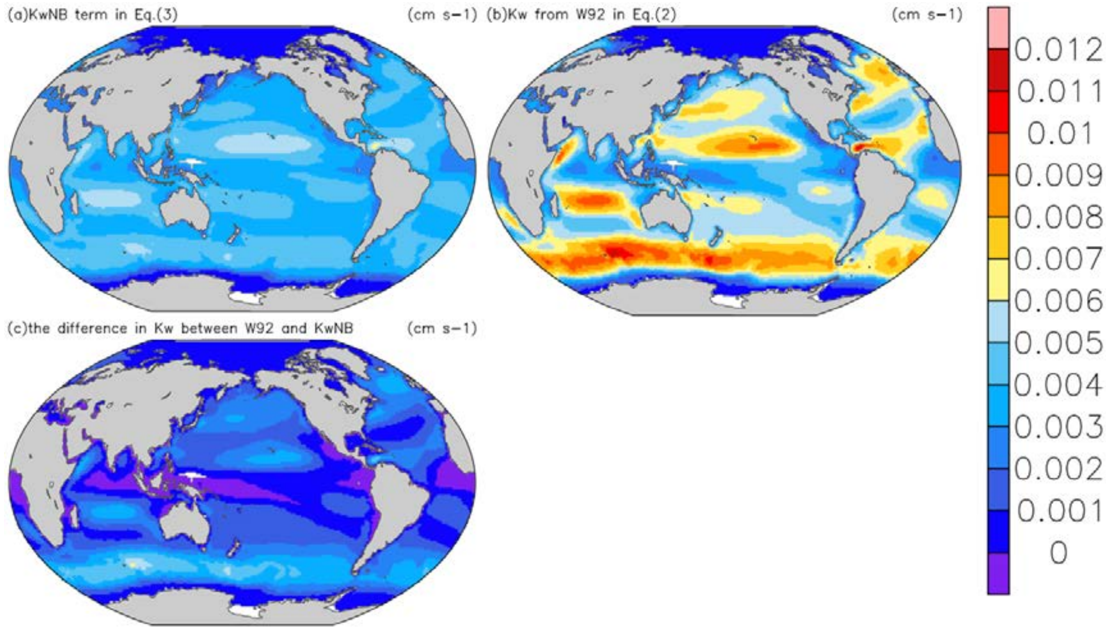

Figure RC1.6.1. The gas transfer velocity from the Eqs. (2–3), (a) the gas transfer velocity of the non-bubble-mediated term ($K_{w,NB}$), (b) K_w from W92 in Eq. (2), and (c) the difference in K_w between W92 and $K_{w,NB}$.

RC1.7. In section 3.1, a figure of the differences would be useful, e.g. B-CTL minus NOAA CT2022 and POP2-waves minus NOAA CT2022.

Response:

Yes, the differences between the model simulation and NOAA CT2022 are now clearly shown, while the original spatial distribution provides the overall positive and negative ranges of CO_2 flux in the model simulation. Please see the revised manuscript and Fig. 2(e–f) for these changes.

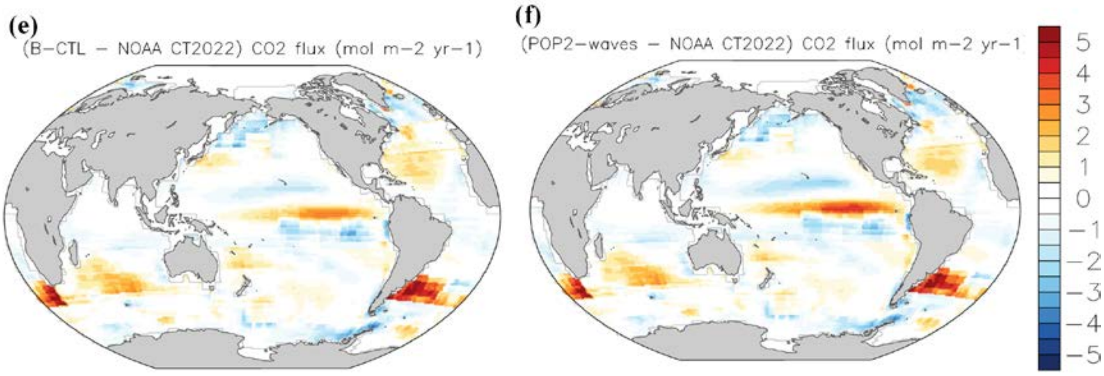

Fig. 2(e–f). Part of Fig. 2 shows the CO_2 flux differences between the model simulation and NOAA CT2022: (e) the difference between B-CTL and NOAA CT2022, and (f) the difference between POP2-waves and NOAA CT2022.

RC1.8. In figures 3, 4 and 5, having the SD in percentage represented by bars makes it very hard to get the idea of the magnitude. It would be better to find the way of having the SD along the flux or K magnitude lines.

Response:

Thank you for your comment. Figure 3 contains 9 subfigures. Plotting ± standard deviation (SD) along the flux or K-magnitude lines for the 3 variables over 12 months would likely produce overlapping curves that are difficult to distinguish. In the revised manuscript, we present the monthly SD values directly, rather than expressing them as a percentage of the overall ranking range in Figs. 3–5, thereby avoiding overlap between the mean lines and SD markers.

RC1.9. Through the results, suddenly the NOAA CT2022 is not used anymore, why? This should be considered as the reference throughout the manuscript, as it is used in Section 3.1.

Response:

We have followed NOAA's Global Monitoring Laboratory usage policy by appropriately acknowledging and citing NOAA CT2022 (Jacobson et al., 2023) as a reference, and we have included acknowledgments throughout the manuscript for providing the CT2022 data.

The inversion CO_2 flux in CarbonTracker CT2022 relies on meteorological fields from that are driven by the daily weather forecasts from the specialized meteorological centers of the world, specifically wind, temperature, pressure, and boundary layer dynamics. In addition, the interannual variability in the

first-guess ocean flux arises entirely from wind-speed effects on gas transfer velocity, because the ocean inversions only retrieve a long-term mean and a smooth trend (Jacobson et al., 2023).

Using alternative reanalysis data (e.g., ERA5, NCEP, or NOAA satellite products) in place of these primary fields may introduce temporal mismatches with CO_2 fluxes, which is inconsistent with the NOAA CT2022 data policy that prescribes the use of only a long-term mean and smooth trend. Consequently, sections 3.2, 3.3, and 3.4 do not attempt to compare the CO_2–meteorology interactions observed in CT2022 with those derived from other reanalysis products.

RC1.10. Please add information about how the different 'regions' mentioned in L188-L196 are selected. Relevant information should be disclosed in the methodology section. Also, why are 12 regions selected first, and then only 9 are used (L197)? Please, provide the necessary explanations.

Response:

Adopting the framework established by Jacobson et al. (2007), NOAA CT2022 partitions the global ocean into 30 basins to represent large-scale circulation and biogeochemical dynamics. This basin-based approach groups regions by their internal coherence in physical processes—such as currents, upwelling, and mixing—and biogeochemical behaviors, including nutrient cycling and carbon uptake. We examined the seasonal variability and mean state of global CO_2 fluxes, excluding regions where flux sign reverses across seasons—an effect that may introduce substantial uncertainty in model–data comparisons—with particular emphasis on the 12 regions exhibiting the strongest oceanic CO_2 fluxes (L188-L196).

Of the 30 regions, those exhibiting seasonal flux sign reversals were excluded, leaving 12 regions for further analysis (L197–L222). These 12 regions are divided into two categories: (1) 9 characteristic regions where the model-simulated CO_2 fluxes are generally consistent with NOAA CT2022 (L197), and (2) 3 regions that exhibit notable discrepancies compared with NOAA CT2022 (L215).

Jacobson, A. R., Gruber, N., Sarmiento, J. L., Gloor, M. and Fletcher, S. E. M.: A joint atmosphere-ocean inversion for surface fluxes of carbon dioxide: I. methods and global-scale fluxes, Global.

Biogeochem. Cy., 21, GB1020, https://doi.org/10.1029/2005GB002556, 2007.

RC1.11. In connection to the previous comment, section 3.2 focuses on the Pacific sink and source regions. Why these regions? Not only the methodological information is needed, but at this point also the overall objective becomes confusing. Are these test cases? Is is the focus of the work to evaluate the global impact of wave and bubble-mediated mechanisms on CO2 flux? Or only focus on certain regions.

Response:

To demonstrate that the sea state–dependent K_w (Deike and Melville, 2018) provides a more suitable estimate of CO_2 flux than the wind-only K_w (Wanninkhof, 1992) under high-wind conditions, we selected two regions with contrasting wind regimes (one with over 30% of U_{10} > 10 m s^{-1} and another with all U_{10} < 10 m s^{-1}). These regions also exhibit stable and significantly positive or negative oceanic CO_2 fluxes, allowing us to compare the correlation between K_w and U_{10}, as shown in Fig. 5 for (a) WP (160–180°E, 35–40°N; Fig. 5a) and (b) EP (230–250°E, 0–5°S; Fig. 5b).

The study also examines the difference between the monthly normal conditions means (Hs < 1.5m) and the K_w derived from averaging daily data with Hs>1.5m, to assess whether the observed phenomenon reported by Gutiérrez-Loza et al. (2022) can also be reproduced in the model. While the relationship between K_w and U_{10}—when based on monthly normal conditions means (Hs < 1.5m) and daily data filtered for Hs>1.5m (enhanced conditions) and then aggregated into 30-year monthly averages—substantially diminishes differences in K_w at the same U_{10}. However, short-term (30-min) observations indicate that K_w can be up to twice as high under similar wind speeds (Gutiérrez-Loza et al., 2022, Fig. 7).

.

RC1.12. It is interesting to assess the impact of waves and bubbles in terms of the total flux (e.g. section 3.3). This has a lot of potential in terms of the relevance of including waves and wave-mediated processes in models to address carbon budgets, but also in terms of the process understanding. Posing questions like is the wave effect equally significant for source and sink regions? What does that represent for the global ocean carbon sink? Does integrating waves into models could bring global carbon sink estimates closer to observational-based estimates? All these questions are incredibly relevant and possible to address in this study.

Response:

We thank the reviewer for recognizing the relevance of this study. We will strive to address key questions regarding the impact of waves on ocean CO_2 flux. The following provides point-by-point responses to the reviewer's questions.

(1) the wave effect equally significant for source and sink regions?

Response:

The wave effect is most pronounced in tropical and subtropical regions, particularly in areas characterized by above-moderate wind speeds but high Hs, such as the tropical central Pacific in the Northern Hemisphere and the tropical Indian Ocean in the Southern Hemisphere, as highlighted by the white dashed borders in Fig. RC1.12.1(b). Additionally, within 30°N–30°S, K_w in the POP2-waves simulation increases by more than 40% relative to B-CTL. This region exhibits both positive and negative CO_2 fluxes but is predominantly a source (positive CO_2 flux).

Comparing Fig. 2(a)–(b) with Fig. RC1.12.1(b) and (d), the wave effect is more pronounced for positive CO_2 flux than for negative CO_2 flux. This is because regions with positive CO_2 flux have a larger air–sea dpCO_2, whereas regions with negative CO_2 flux have a smaller dpCO_2. As a result, the multiplicative effect enhances the impact of POP2-waves more strongly in regions with positive CO_2 flux.

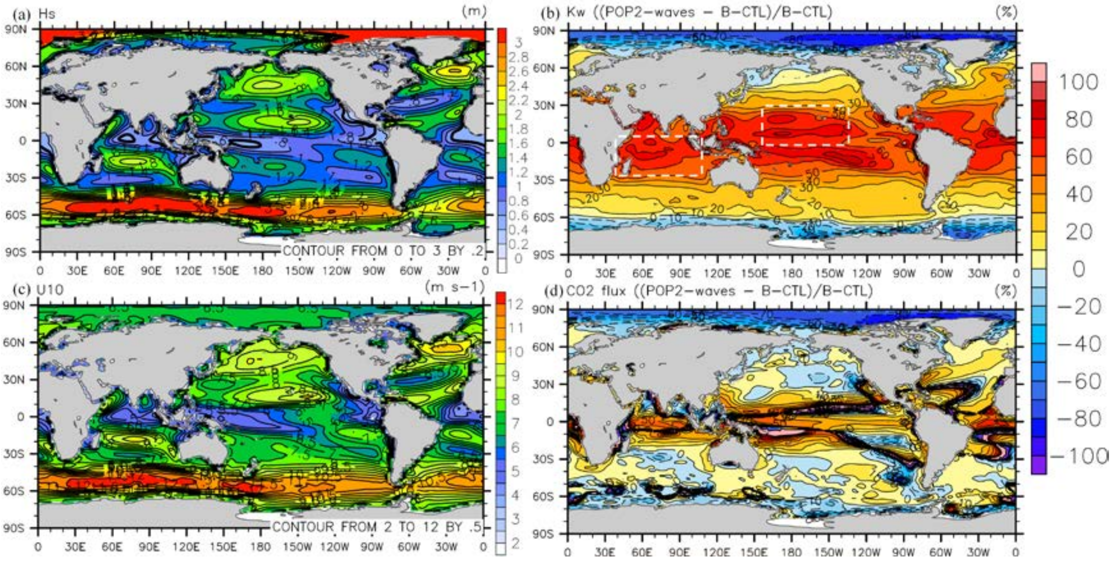

Figure RC1.12.1. Thirty-year mean fields of (a) significant wave height (Hs), (b) the difference in gas transfer velocity (K_w) between POP2-waves and B-CTL, (c) 10-m wind speed (U_{10}), and (d) the difference in CO_2 flux between POP2-waves and B-CTL. The white dashed borders in panel (b) highlight regions with larger K_w differences associated with higher Hs and U_{10}.

(2) What does that represent for the global ocean carbon sink?

Response:

As noted in the conclusion, under the $dpCO_2$-driven negative feedback associated with the interaction between CO_2 fluxes and the carbonate–pH system, POP2-waves show increases of 11.8%, 41.6%, and 1.8% in the negative CO_2 flux regions, positive CO_2 flux regions, and the global ocean carbon sink, respectively, compared to B-CTL.

(3) Does integrating waves into models could bring global carbon sink estimates closer to observational-based estimates?

Response:

Overall, incorporating waves into the model can bring global carbon sink estimates closer to NOAA CT2022. However, because it increases both positive and negative CO_2 flux regions globally, the net change in the global carbon sink is only 1.8%, due to the compensating effects between positive and negative contributions.

RC1.13. While the results focus on the 'kinematic' part of the flux, assessing the effect of waves and bubbles on the gas exchange, the discussion section largely focuses on the 'thermodynamic' component of the flux, and the links between physics and biogeochemistry. Large parts of the discussion are written as introductory concepts (e.g. L334- 338), of course, because previously the focus was on the kinematic properties (i.e. waves, bubbles, wind, u, Kw, etc.). Other parts are largely written as results, describing additional figures and introducing new findings, correlations, uncertainty analysis. Despite being interesting, all this is not a discussion. I encourage the authors to reconsider the key objectives and structure of the manuscript.*

Response:

Thank you for your comment. Completing this interdisciplinary manuscript was challenging. It required programming expertise to port the wave module from other models into the CESM1 framework, as well as effective coupling between the wave, atmosphere, sea ice, and ocean components. The study also involved concepts from kinematics, thermodynamics, and biogeochemistry. All of the coding and most of the writing were carried out by the first author, I also aimed to clearly explain the underlying physical principles to make the manuscript as complete as possible.

The primary contribution of this study lies in its online coupling framework, which explicitly incorporates wave effects into air–sea CO_2 flux simulations,

thereby capturing the ocean's buffering capacity. In contrast, treating $dpCO_2$ and wave-induced K_w independently leads to a substantial overestimation of air–sea CO_2 fluxes when compared to online coupling POP2-waves simulations (section 4.3).

Lines 334–338 have been rewritten as follows:

The marine carbonic acid system is a nonlinear, coupled system governed by CO_2 dissolution equilibrium, ($CO_{2(aq)} + H_2O \overset{K_H}{\leftrightarrow} H_2CO_{3(aq)}$), where the Henry's constant (K_H) for CO_2 in water at 25°C is approximately 3.4 x 10^{-2} (m/atm), two-step dissociation reactions, and the conservation of the total dissolved inorganic carbon (DIC) and total alkalinity (TA), ultimately determining pH and the distribution of carbonate species. The H_2CO_3 has two hydrogen ions and dissociates in two steps:

$$H_2CO_3 \overset{K_{a1}}{\longleftrightarrow} H^+ + HCO_3^- \qquad K_{a1} = 4.4\times10^{-7} \tag{4}$$

$$HCO_3^- \overset{K_{a2}}{\longleftrightarrow} H^+ + CO_3^{2-} \qquad K_{a2} = 4.7\times10^{-11} \tag{5}$$

The DIC can be expressed as:

$$\begin{aligned} DIC &= [H_2CO_3] + [HCO_3^-] + [CO_3^{2-}] \\ &= K_H pCO_2^w + \frac{K_{a1} K_H pCO_2^w}{[H^+]} + \frac{K_{a1} K_{a2} K_H pCO_2^w}{[H^+]^2} \\ &= K_H pCO_2^w \left(1 + \frac{K_{a1}}{[H^+]} + \frac{K_{a1} K_{a2}}{[H^+]^2}\right) \\ &= K_H pCO_2^w ([H^+]^2 + K_{a1} [H^+] + K_{a1} K_{a2})/[H^+]^2 \end{aligned} \tag{6}$$

The marine carbonate system describes the distribution of DIC among its chemical species in seawater and is jointly governed by TA and pH. From Eq. (6), if the oceanic pCO_2^w and pH are known, the DIC can be determined, conversely, pCO_2^w can be inferred from DIC. TA is defined as the sum of the proton-neutralizing capacities of all weak acid anions in seawater (Dickson, 1981) and can be expressed as:

$TA=[HCO_3^-]+2[CO_3^{2-}]+[B(OH)_4^-]+[OH^-]+[HPO_4^{2-}]+2[PO_4^{3-}]+[SiO(OH)_3]+[NH_3]+[HS^-]-[H^+]-[H_3PO_4]$. In the POP2-waves framework, TA, pH and biogeochemistry are also used to calculate pCO_2. The biogeochemical module of POP2 (MARBL) updates TA in each grid cell by solving a coupled transport–reaction equation (Long et al., 2021). The average pH of the ocean is currently around 8.1 (Fig. 8c), reflecting slightly alkaline conditions. Within the DIC system,

bicarbonate ions (HCO_3^-) are the dominant species because the prevailing pH lies between pK_{a1} and pK_{a2}. However, continued uptake of atmospheric CO_2 drives a decline in pH, a process termed ocean acidification.

We have clarified the key objectives and revised the manuscript structure accordingly. Please refer to the updated version for these changes.

Reference

Dickson, A. G.: An exact definition of total alkalinity and a procedure for the estimation of alkalinity and total inorganic carbon from titration data, Deep-Sea Res., 28A (6), 609-623, https://doi.org/10.1016/0198-0149(81)90121-7, 1981.

Long, M. C., Moore, J. K., Lindsay, K., Levy, M., Doney, S. C., Luo, J. Krumhardt, K. M., Letscher, R. T., Grover, M., and Sylvester, T.: Simulations with the marine biogeochemistry library (MARBL). J. Adv. Model. Earth Sy., 13(12), e2021MS002647. https://doi.org/10.1029/2021MS002647, 2021.

RC1.14. In the conclusions, the authors point to significant challenges in the POP2-waves coupling. However, these are not described or discussed in the paper. It is also mentioned that the results are used to compare CO2 fluxes (including wave and bubble-mediated effects) with NOAA CT2022, but this is only very briefly done. The conclusions must be consistent with the content of the rest of the manuscript.

Response:

Coupling a wave model into an ocean circulation model to simulate air–sea CO_2 flux presents substantial challenges arising from multi-scale physical processes, cross-component coupling, and nonlinear carbon cycle feedbacks. These challenges can be categorized into three main aspects: model coupling and implementation, underlying theoretical processes and data analysis (kinematics, thermodynamics, and biogeochemistry), and model validation and uncertainty.

Figure 11 consolidates key findings from previous sections to synthesize the regions of maximum negative and positive air–sea CO_2 flux (WP: 160–180°E, 35–40°N and EP: 230–250°E, 0–5°S, respectively), organized by winter and summer. As detailed in Section 3.1, the figure summarizes the mean and seasonal variations in air–sea CO_2 flux. Furthermore, it incorporates the changes in pCO_2^w and pH between the POP2–waves and B–CTL experiments (described in Section 4.1 and shown in Fig. 8), illustrating how the coupled model reduces high pCO_2^w by over 10 ppm in the EP and induces pH

differences of approximately ±0.01. Finally, Fig. 11 includes thermodynamic SST information, with colors highlighting the contrasts between the WP and EP regions, thereby illustrating the relationship between air–sea CO_2 flux and SST described in Section 4.2 and Fig. 9c.

Technical corrections:

RC1.15. Use 'biogeochemistry' not 'geochemistry'

Response:

Thank you for your comment. Please see revised manuscript for the change.

RC1.16. Use 'air-sea flux' instead of 'sea-air flux'

Response:

Thank you for your comment. Please see revised manuscript for the change.

RC1.17. L55: 'slow conduction' can be removed from the sentence has here the main topic is on mass transport which under non-turbulent conditions 'occurs through molecular diffusion'.

Response:

We have removed 'slow conduction' from the sentence. Please see revised manuscript for the change.

RC1.18. L55: Avoid using 'sources and sinks of CO2 flux'. Either refer to a region as a 'source or sink of CO2', or use 'positive or negative CO2 flux', but there is no such thing as a source or sink of the flux.

Response:

We use "sources and sinks" to refer to an increase in magnitude in both positive and negative CO_2 flux regions. Here, "positive" and "negative" indicate only the direction of air–sea $dpCO_2$, i.e., from the ocean to the atmosphere or vice versa. For example, the CO_2 flux simulated by POP2-waves is stronger than that of B-CTL across both positive and negative CO_2 flux regions.

We have removed the phrase "sources and sinks of CO_2 flux" and replaced it with "positive or negative CO_2 flux," except in the cases described above, where "and" is used to indicate enhancement in both regions.

RC1.19. L179: 'mean air-sea CO2 flux' or 'mean atmosphere-ocean CO2 flux' instead of 'mean ocean CO2 flux'.

Response:

Thank you for your comment. Please see revised manuscript for the change.

Anonymous Referee #2 (pp.14–30)
The reviewer comments are formatted in italics and the authors response to the comments are formatted in bold.
Notation *RC2.P#* represents Reviewers Comment. Paragraph Number

Specific comments:

RC2.1 L26/Figure 9: The interpretation of the regressions should consider the flux direction. The sign convention in this paper assumes that ocean outgassing is positive, so it's positively correlated with kw, while ocean uptake is negatively correlated with kw; however, its magnitude may still be enhanced, if not more so. Consider providing more interpretation than simply stating correlations. For example, kw and SST are negatively correlated because they reflect the latitudinal structure of colder ocean waters and more intense sea states.

Response:

To confirm the statistical significance of the variables, we first conducted a t-test (at the 95% confidence level). Subsequently, we standardized both the air–sea CO_2 flux and the relevant variables (air–sea $dpCO_2$ (Fig. 9a), $K_{w,660}$ (Fig. 9b), SST (Fig. 9c), and pH (Fig. 9d)) into anomalies with a mean of 0 and a standard deviation of 1, thereby removing the influence of differing units and enabling comparison on a common scale. This allows the LRC to range between −1 and +1.

In the revised manuscript, we have added the following explanation to clarify the relationship between air–sea CO_2 flux and sea state: $K_{w,660}$ and SST are negatively correlated, reflecting the latitudinal gradient where colder, high-latitude waters are associated with more intense sea states and higher $K_{w,660}$. This pattern occurs because lower temperatures in high-latitude regions increase CO_2 solubility, thereby enhancing oceanic uptake. Conversely, higher temperatures in tropical regions reduce solubility, promoting CO_2 outgassing. As SST increases, CO_2 molecules become more mobile in seawater, enhancing diffusion and reducing the Schmidt number (Sc=ν/D, the ratio of kinematic viscosity to the diffusion coefficient). Because K_w is parameterized as $Sc^{-0.5}$, a decrease in Sc leads to an increase in $K_{w,660}$ and air–sea CO_2 flux.

RC2.2 L37: Consider adding a line that makes the flux direction convection explicit, clearly stating that positive fluxes are ocean outgassing to the atmosphere.

Response:

Thank you for your suggestion. Please see the revised manuscript for the change.

RC2.3. L44/L139/L230: I believe the equation you're showing is from Wanninkhof (2014), not from Wanninkhof (1992). Please modify here and elsewhere. Please add that the 10 m wind speed is the neutral wind speed.

Response:

Thank you for pointing out the mistake. In the B-CTL control experiment, the coefficient (*k*) for gas transfer velocity in Equation (2) follows Wanninkhof (1992), where k = 0.31. I mistakenly entered 0.251, which may have led to confusion with Wanninkhof (2014); this has now been corrected in the revised manuscript. For further details, please refer to the original CESM1 POP2 code (ecosys_mod.F90), specifically the annotation of the variable *xkw_coeff* (! a = 0.31 cm/hr s^2/m^2 in (s/cm)) and Table RC1.1.

In the revised manuscript, Eq. (2) includes an additional symbol description: U_{10}^2 represents the squared neutral mean wind speed at 10 m above the surface.

Table RC1.1 The coefficient (*k*) used to parameterize gas transfer velocity ($K_{w,660}$) differs between Wanninkhof (1992) and Wanninkhof (2014).

	Wanninkhof (1992)	Wanninkhof (2014)
the coefficient (*k*) of gas transfer velocity ($K_{w,660}$) $K_{w,660} = k <U_{10}^2> (Sc/660)^{-0.5}$	0.31	0.251
optimal method	applicable to deduce $K_{w,660}$ at steady winds	The optimal coefficient was obtained using an inverse modeling approach with CCMP[1] winds and the Modular Ocean Model General Circulation Model (MOM3 GCM).

Note:[1]CCMP: The Cross-Calibrated Multi-Platform (CCMP) are produced by Remote Sensing Systems (RSS) with support from a NASA Ocean Vector Winds Science Team grant.

RC2.4. Rustogi et al. (2025) used an ocean circulation model to quantify wave-bubble effects on CO2. Might be a relevant reference.

Response:

We thank the reviewer for the helpful suggestion to better clarify the model framework. Rustogi et al. (2025) employs a fully coupled ocean–biogeochemistry modeling system based on the MOM6 ocean circulation model and the COBALTv2 biogeochemical module. This framework simulates ocean dynamics, temperature, and carbon cycling processes including dissolved inorganic carbon (DIC), pCO_2, and wave effects in the air–sea CO_2 exchange. They also describe a nonlinear pCO_2 feedback mechanism within the coupled ocean–carbon system that regulates air–sea CO_2 flux.

Rustogi et al. (2025) also indicate that as pCO_2^w responds to changes in DIC and alkalinity, the air–sea $dpCO_2$ is partially reduced. This induces a negative feedback loop, whereby enhanced CO_2 uptake (or outgassing) is damped by chemical re-equilibration within the marine carbonate system, consistent with the findings of this study. Furthermore, Wu et al. (2025) also investigated the influence of these mechanisms within a global ocean coupled model, aiming to better capture the indirect effects of changes in surface DIC—driven by air–sea CO_2 flux—on the flux itself.

Reference

Rustogi, P., Resplandy, L., Liao, E., Reichl, B. G., and Deike, L.: Influence of wave-induced variability on ocean carbon uptake. Global Biogeochem. Cy., 39, e2024GB008382. https://doi.org/10.1029/2024GB008382, 2025.

Wu, L., Cai, Y., and Rutgersson, A.: Ocean surface waves impact on global air-sea CO_2 flux, Biogeochem., 168, 68, https://doi.org/10.1007/s10533-025-01267-y, 2025.

RC2.5. Data, model experiments, and methodology: I agree with the other reviewer that there isn't sufficient information to understand how the model was spun up, how wave properties through coupling lead to the significant wave height variable, and about the individual model components, such as the biogeochemical module. Please also add information about how wind friction is calculated, as it's used in the wave-bubble formulation. Perhaps more details can be added to Figure 1, which is currently not very informative and, in its current form, should be moved to the supplementary material.

Response:

Thank you for your suggestion. We have substantially revised the methodology section of the manuscript, including (1) the development of the CESM1–POP2–waves model and its component modules (Sections 2.1 and 2.2), (2) a more detailed description of CarbonTracker (Section 2.3), (3) additional information on POP2–waves input data and atmospheric forcing (Sections 2.1 and 2.2), and (4) an expanded description of the Marine Biogeochemistry (MARBL) module in Section 2.1 and Fig. 1, highlighting that all components influence the air–sea CO_2 flux. Please refer to the revised manuscript for details of these changes.

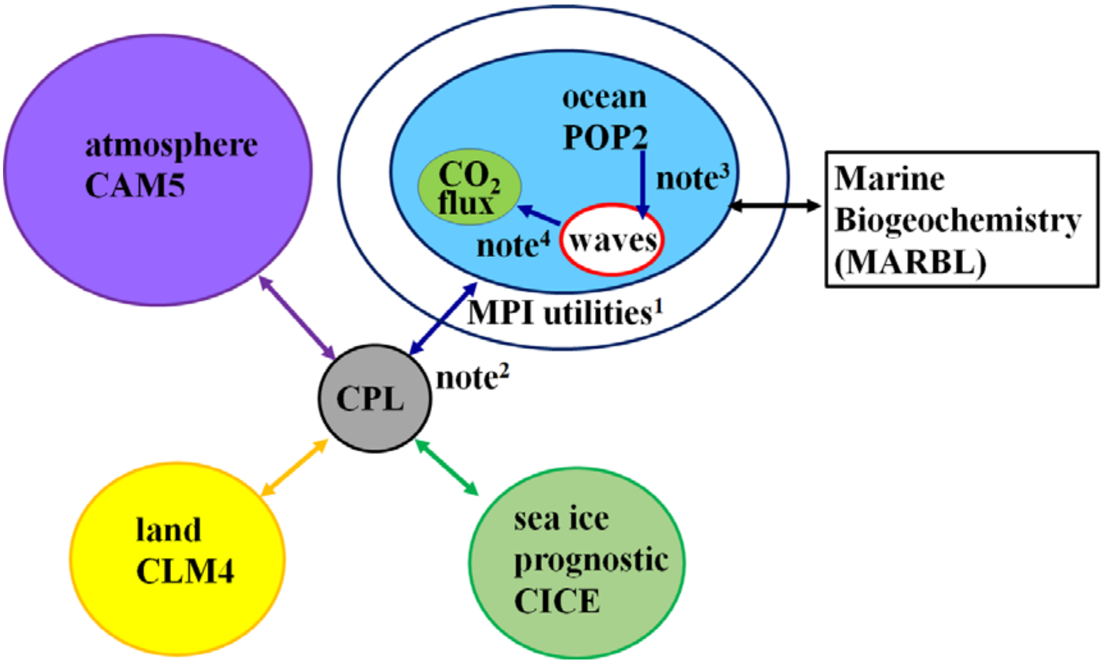

Figure 1. Architecture diagram for POP2–waves experiment in CESM1.2.2 framework, all components adhere to the CESM 1.2.2 framework, except for certain parts of the ocean component. The model components including components for the atmosphere [Community Atmosphere Model version 5 (CAM5)], land [Community Land Model version 4 (CLM4)], ocean [Parallel Ocean Program, version 2 (POP2)], along with its associated modules—the

waves module (waves) and the Marine Biogeochemistry (MARBL) module—sea ice [prognostic Los Alamos Sea Ice Model (CICE)], and the coupler (CPL).

Note:
[1]The wave-module variables are communicated between neighboring blocks via MPI, including zonal and meridional 10-m winds, wave radiation stress, subsurface momentum, and wave radiation and energy densities.
[2] To transfer variables such as zonal and meridional 10-m winds and friction velocity (including sea surface and ice fraction) from the CPL to POP2.
[3] The wave module receives variables from POP2, including the interpolation of depth-varying currents from z-coordinates (60 levels) to the wave module's vertical sigma coordinates (21 levels), along with ocean grid information in the x, y, and z directions.
[4] The wave module outputs significant wave height and friction velocity from the CPL for calculating the bubble-mediated gas transfer velocity in Eq. (3).

This study follows the NCAR CESM1 framework, in which the default friction velocity (u^*) is computed in the coupler (CPL) as part of the bulk aerodynamic formulation for air–sea momentum exchange. The friction velocity is derived from the surface wind stress and air density (Craig et al., 2012) as:

$$\boldsymbol{u}^* = \sqrt{\frac{|\boldsymbol{\tau}|}{\boldsymbol{\rho_a}}}$$

Where τ is the surface wind stress vector (N m^{-2}) and ρ_a is the near-surface air density (kg m^{-3}). The magnitude of the wind stress (τ) is often parametrized as a function of wind speed at a 10-m height above the surface in the form:

$$\boldsymbol{\tau} = \boldsymbol{\rho_a C_D u_{10}^2}$$

Where ρ_a is the density of the surface air and C_D is a dimensionless wind drag coefficient which depends on atmospheric stability and surface roughness. In CESM1, the drag coefficient C_D is computed within the atmospheric boundary layer scheme (e.g., based on Monin–Obukhov similarity theory), and the resulting stress is passed through the coupler (CPL) to the ocean and sea ice components. Thus, the friction velocity used by ocean and wave-related parameterizations in CESM1 is dynamically consistent with the atmospheric forcing and surface exchange physics.

Reference

Craig, A. P., Vertenstein, M., and Jacob, R.: A new flexible coupler for Earth system modeling developed for CCSM4 and CESM1, Int. J. High Perform. Comput. Appl., 26(1), 31–42, doi:10.1177/1094342011428141, 2012.

RC2.6. L155: Equation 3 is missing a Schmidt term in the symmetric bubble gas exchange formulation. Please check the original publication. I'd suggest updating the formulation to the new generalized formulation proposed by Deike et al. (2025), which includes updated coefficients and an asymmetric bubble flux contribution, expected to have a small impact on CO2 but potentially significant for O2 fluxes.

Response:

We have added the Schmidt number term to the symmetric bubble gas exchange in Eq. (3). Deike et al. (2025) show that the wind–wave–bubble formulation explicitly decomposes gas exchange into nonbreaking, symmetric bubble, and asymmetric bubble components, introducing a physically based asymmetric bubble term that drives a unidirectional flux into the ocean independent of the air–sea $dpCO_2$. This framework emphasizes the process-level physics of bubble-mediated exchange and highlights the roles of gas solubility and bubble dynamics, particularly under energetic sea states.

We appreciate the suggestion to adopt this generalized formulation; however, implementing Deike et al. (2025) would require rerunning the simulations, which is not feasible at this stage as it would take more than one month to complete. As part of the ongoing development of a new biogeochemistry model within the CESM3 framework, we plan to implement the wind–wave–bubble parameterization of Deike et al. (2025). The updated model will be evaluated and compared with the present findings in a forthcoming manuscript.

RC2.7. L181/L184: These statements need more depth - what is consistent and what isn't? Perhaps adding global integrals values can help quantify if adding waves improves the match with the NOAA product. I agree with the other reviewer that adding difference plots may be more informative at least when comparing model simulations.

Response:

We further clarify the agreements and discrepancies in air–sea CO_2 flux among POP2-waves, B–CTL, and NOAA CT2022 in Section 3.1 and Figs. 3 and 4. The differences (B–CTL minus NOAA CT2022 and POP2-waves minus NOAA CT2022) are also shown in Fig. 2e–f. We do not use global integrals; instead, we analyze the 30-year monthly variability in the model simulations and the 20-year variability in NOAA CT2022, along with their standard deviations.

RC2.8. Figure 3: It isn't evident what this figure is demonstrating. The seasonal cycles vary between the product and coupled simulations across regions. If the point is to compare with the observation-based reference, then it's useful to continue that analysis throughout the manuscript; otherwise, it may be more informative to focus largely on the differences among the model simulations, since they are internally self-consistent. One interesting question would be to evaluate the difference in the carbon inventory in the ocean interior.

Response:

Thank you for your comment. Figure 3 presents the seasonal cycles of air–sea CO_2 flux, comparing product-based and coupled simulations across regions, as well as their differences relative to NOAA CT2022. The blue solid line represents NOAA CT2022, the black dashed line represents B–CTL, and the red solid line represents POP2–waves; the corresponding standard deviations are shown as bar graphs in the same colors.

Our experimental design focuses on air–sea carbon exchange at the interface, with limited output of broader carbon system variables. Ocean carbon inventory was not included in the initial design; however, it may be incorporated in future CESM3-based biogeochemical model development and experiment design.

RC2.9. Results: The results also include discussion material (e.g., L203-206, L282-283). In general, hard to understand the results without referencing the figures, and the text includes a lot of details about what the figures show, without interpreting the findings. Consider streamlining the key findings.

Response:

We have moved the discussion of Fay et al. (2024) to Section 4.2 and simplified the content in Lines 203–206 as follows. In the revised manuscript, the black dashed line and the red and blue solid lines represent the monthly means of B–CTL, POP2–waves, and NOAA CT2022, respectively, and the corresponding standard deviations are shown as bar graphs in the same colors.

We have revised the ambiguous wording in Lines 282–283 as follows. Johansson et al. (2022) reported that significant wave height generally increases with wind speed, but the relationship is strongly modulated by wind direction and regional conditions, leading to spatially variable and nonlinear wind–wave coupling.

Reference

Fay, A. R., Munro, D. R., McKinley, G. A., Pierrot, D., Sutherland, S. C., Sweeney, C., and Wanninkhof, R.: Updated climatological mean ΔfCO_2 and net sea–air CO_2 flux over the global open ocean regions, Earth Syst. Sci. Data, 16, 2123–2139, https://doi.org/10.5194/essd-16-2123-2024, 2024.

Johansson, M. M., Björkqvist, J.-V., Särkkä, J., Leijala, U., and Kahma, K. K.: Correlation of wind waves and sea level variations on the coast of the seasonally ice-covered Gulf of Finland, Nat. Hazards Earth Syst. Sci., 22, 813–829, https://doi.org/10.5194/nhess-22-813-2022, 2022.

RC2.10. Figure 5: The standard unit for kw is cm/hr - please update in this figure and elsewhere (Figure 7, L296). It isn't clear why the analysis shifts to focus on two regions (WP and EP) that weren't explicitly indicated by the masks in Figure 2.

Response:

We have converted $K_{w,660}$ to the standard unit (cm hr^{-1}) in Figs. 5 and 7 and in Line 296. Xu et al. (2022) indicate that, in CMIP6 models, the Atlantic Ocean exhibits regionally varying SST biases arising from both dynamical and thermodynamical limitations, while the Southern Ocean shows a persistent warm bias, a well-known issue in many Earth system models. We exclude these regions to focus on how strong wave effects influence $K_{w,660}$ and air–sea CO_2 exchange in areas with the most pronounced positive or negative fluxes. The WP region (160–180°E, 35–40°N) exhibits the strongest negative air–sea CO_2 flux within the NWP (Fig. 2d), whereas the EP region (230–250°E, 0–5°S) within the EEP (Fig. 2d) exhibits the strongest positive air–sea CO_2 flux. Table RC2.10.1 provides a comparison of the corresponding mean air–sea CO_2 flux values.

Table RC2.10.1 Mean air–sea CO_2 fluxes in regions with the most pronounced positive and negative values (mol m^{-2} yr^{-1}).

Positive air–sea CO_2 fluxes		Negative air–sea CO_2 fluxes	
EP (230–250°E, 0–5°S)	EEP in Fig. 2d	WP (160–180°E, 35–40°N)	NWP in Fig. 2d
3.7	1.8	-3.9	-3.0

Reference

Xu, G., Chang, P., Ramachandran, S., Danabasoglu, G., Yeager, S.,

Small, J., Zhang, Q., Jing, Z., and Wu, L.: Impacts of Model Horizontal Resolution on Mean Sea Surface Temperature Biases in the Community Earth System Model, J. Geophys. Res.-Oceans, 127, e2022JC019065, https://doi.org/10.1029/2022JC019065, 2022.

RC2.11. Figure 6: Consider adding wind speed distribution to better distinguish modeled responses.

Response:

In Fig. 6, we examine the relationship between air–sea CO_2 flux and U_{10} under high-wind conditions (U10 > 10 m s^{-1}) in the Western Pacific (160–180°E, 35–40°N), with regression lines shown for (a) B–CTL and (b) POP2–waves. As indicated in Fig. 5a, there is a significant difference in $K_{w,660}$ between POP2–waves and B–CTL under U_{10} > 10 m s^{-1} in this region. The x-axis in Fig. 6 shows the wind speed distribution. Overall, U_{10} and the negative air–sea CO_2 flux exhibit a linear relationship, with a stronger correlation in POP2–waves (R=0.48) than in B–CTL (R=0.35), indicating that the wave-related $K_{w,660}$ under high-wind conditions better captures air–sea CO_2 flux variability in this region.

.

RC2.12. Figure 7: The figure doesn't show the surface circulation or the Hs fields as stated in the text. The Kw from the ctrl experiment and the kwNB from the wave experiment aren't directly comparable, so if the point is to compare the two, it should be the total kw, and perhaps their difference. Could you comment on the kw pattern in panel c: it lacks the structure seen across products and modeled fluxes (e.g., Reichl and Deike, 2020) – is it related to the coupling? Are there other references that demonstrate that the kw/flux structure is CESM-specific?

Response:

Thank you for pointing out the mistake. In Fig. 7a, the shaded areas represent the near-surface atmospheric condition of 10-m wind speed (U_{10}, m s^{-1}), with contours indicating sea level pressure (PSL, mb). Figure 7b shows the H_s fields with contours, as described in Lines 283–286 of the original manuscript. This clarifies the relationship between the H_s fields and the ratio of $K_{wB,660}$ to $K_{w,660}$ described in the text.

We changed the contours in Fig. 7d to represent the difference ($K_{wNB,660}$–$K_{wB,660}$) in cm hr^{-1}, illustrating the difference in gas transfer velocity between the non-bubble ($K_{wNB,660}$) and bubble ($K_{wB,660}$) components under different spatial distributions of $u*$ (Fig. 7b) and U_{10} (Fig. 7a).

Since the percentage ratio of $K_{w,660}$ ((POP2–waves−B–CTL)/B–CTL) is unclear and does not adequately represent the magnitude of the difference between POP2–waves and B–CTL, we changed the contours in Fig. 7c to show the absolute difference in $K_{w,660}$ (POP2–waves − B–CTL) in cm hr^{-1}.

Figure 7c shows that the larger differences in $K_{w,660}$ (POP2–waves − B–CTL) are mainly distributed in regions with higher H_s, particularly within 30°N–30°S. Although wind speeds in the Indian Ocean and tropical Pacific are relatively low (< 5 m s^{-1}; Fig. 7a), the $K_{w,660}$ values in POP2–waves are still about 9 cm hr^{-1} higher than those in B–CTL. In these regions, the POP2-waves enhanced $K_{w,660}$ is primarily dominated by the non-bubble-mediated component, as shown in Fig. 7d. Although H_s is also large in the Southern Ocean (Fig. 7b), it does not contribute substantially to the $K_{w,660}$ difference between POP2–waves and B–CTL because the high U_{10} in this region (Fig. 7a) already produces large $K_{w,660}$ values through the empirical formulation of Wanninkhof (1992).

Compared with Reichl and Deike (2020), this study presents the climatological U_{10} as shaded colors in Fig. 7a using a high-contrast color bar, showing patterns similar to those in Fig. 1d of Reichl and Deike (2020), despite their use of a single-color scale. This study also presents climatological H_s contours in Fig. 7b, which are similar to those shown in Fig. 1e of Reichl and Deike (2020). Both studies exhibit common features, with high U_{10} and H_s values distributed over the North Pacific around 30°–50°N, the Indian Ocean around 10°–20°S, and the Southern Ocean. Because $K_{w,660}$ is strongly influenced by both U_{10} and H_s, the spatial distribution of B–CTL $K_{w,660}$ (shaded) and the contours difference $K_{w,660}$ (POP2–waves − B–CTL) shown in Fig. 7c is also similar to Fig. 1f of Reichl and Deike (2020), which indicated in Fig. RC2.12.1.

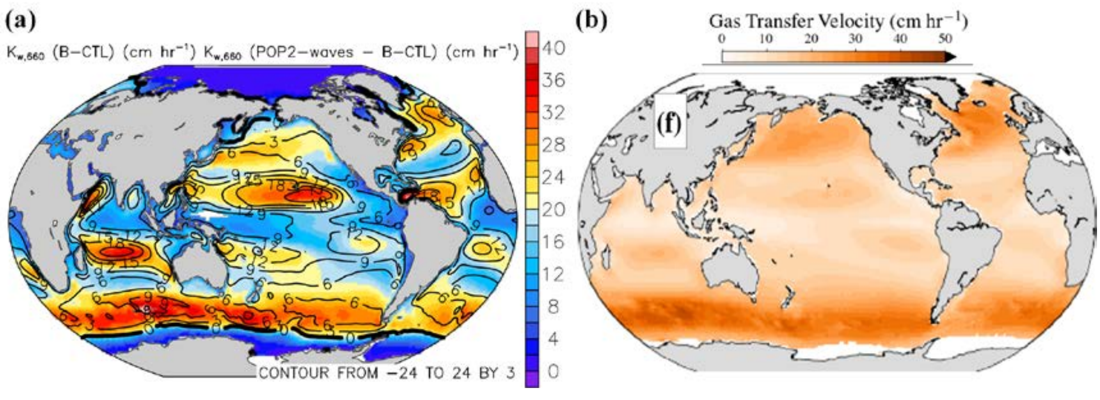

RC2.12.1. Comparison of $K_{w,660}$ between this study and Reichl and Deike (2020):

(a) Fig. 7c in this manuscript and (b) Fig. 1f in Reichl and Deike (2020).

RC2.13. L290: There shouldn't be a discrepancy in the Ab coefficient between this study and Reichl and Deike's formulation, since that's what is used here. Perhaps the differences have more to do with the tool?

Response:

Yes, the A_B coefficients follow the formulation suggested by Reichl and Deike (2020). The ratio of $K_{wB,660}/K_{w,660}$ in POP2–waves can be expressed as follows:

$$\frac{K_{wB,660}}{K_{w,660}} = \frac{\frac{A_B}{K_0\,R\,T_0} u_*^{\frac{5}{3}}\,(g\,H_S)^{\frac{2}{3}}\left(\frac{Sc}{660}\right)^{-\frac{1}{2}}}{A_{NB} u_* \left(\frac{Sc}{660}\right)^{-\frac{1}{2}} + \frac{A_B}{K_0\,R\,T_0} u_*^{\frac{5}{3}}\,(g\,H_S)^{\frac{2}{3}}\left(\frac{Sc}{660}\right)^{-\frac{1}{2}}} \qquad \text{(RC2.13.1)}$$

When the Schmidt number term is removed, the ratio of $K_{wB,660}/K_{w,660}$ can be expressed as follows:

$$\frac{K_{wB,660}}{K_{w,660}} = \frac{\frac{A_B}{K_0\,R\,T_0} u_*^{\frac{5}{3}}\,(g\,H_S)^{\frac{2}{3}}}{A_{NB} u_* + \frac{A_B}{K_0\,R\,T_0} u_*^{\frac{5}{3}}\,(g\,H_S)^{\frac{2}{3}}} \qquad \text{(RC2.13.2)}$$

Compared with Reichl and Deike (2020), the constant coefficients are the same; therefore, after substituting the numerical values of A_{NB} (1.55 ×10^{-4}, no dimension), A_B (1.2 ×10^{-5} s^2 m^{-2}), R (0.082 L atm mol^{-1} K^{-1}), and g (9.806 m s^{-1}) and simplifying, the ratio $K_{wB,660}/K_{w,660}$ can be expressed as follows:

$$\frac{K_{wB,660}}{K_{w,660}} \propto \frac{4.32\,\frac{1}{K_0\;T_0} u_*^{\frac{5}{3}}\,(H_S)^{\frac{2}{3}}}{u_* + 4.32\,\frac{1}{K_0\;T_0} u_*^{\frac{5}{3}}\,(H_S)^{\frac{2}{3}}} \propto \frac{4.32\,\frac{(u_* H_S)^{\frac{2}{3}}}{K_0\;T_0}}{1 + 4.32\,\frac{(u_* H_S)^{\frac{2}{3}}}{K_0\;T_0}} \qquad \text{(RC2.13.3)}$$

The main difference in the ratio $K_{wB,660}/K_{w,660}$ between Reichl and Deike, (2022) and this study lies in $\frac{(u_* H_S)^{\frac{2}{3}}}{K_0\;T_0}$. Table RC2.13.1 summarizes the differences in the sources of the parameters used in Eq. RC2.13.3.

Table RC2.13.1 The differences in the sources of the parameters between Reichl and Deike, (2020) and POP2-waves

item	Reichl and Deike, (2020)	POP2-waves (this study)
T_0 (SST)	T_0 derived from satellite observations	T_0 is obtained from POP2 simulations
H_s (significant wave height)	H_s simulated with WAVEWATCH III	H_s is generated by the POM wave module coupled within the POP2 system
k_0 (solubility constant)	The empirical relationship of Weiss (1974)	The empirical relationship of Weiss (1974)
u* (friction velocity)	u* estimated from U_{10} using the bulk parameterization of	u* is computed in the coupler as part of the bulk

	Edson et al, (2013)	**aerodynamic formulation for air–sea momentum exchange**

Since the sources of the $K_{w,660}$ parameters (T_0, H_s, and u*) differ substantially, the spatiotemporal distribution of $\frac{(u_* H_S)^{\frac{2}{3}}}{K_0\ T_0}$ also differs between Reichl and Deike, (2020) and this study. The bubble contribution to the total gas transfer velocity ($K_{wB,660}/K_{w,660}$) in POP2–waves is approximately 38%, which is slightly higher than ~30% reported by Reichl and Deike (2020).

Reference

Edson, J. B., Jampana, V.,Weller, R. A., Bigorre, S. P., Plueddemann, A. J., Fairall, C.W., Miller, S. D., Mahrt, L., Vickers, D., and Hersbach, H.: On the exchange of momentum over the open ocean. J. Phys. Oceanogr., 43, 1589 – 1610, https://doi.org/10.1175/JPO-D-12-0173.1, 2013.

> *RC2.14. L310: This point is not sufficiently demonstrated in your study - there is only a brief mention of changes in pH in two ocean regions. Either remove or restructure results to show this.*

Response:

We removed the description in L310–315 and restructured the results after introducing the marine carbonate system related to pH and total alkalinity in Section 4.1.

The marine carbonic acid system is a nonlinear, coupled system governed by CO_2 dissolution equilibrium, ($CO_{2(aq)} + H_2O \overset{K_H}{\leftrightarrow} H_2CO_{3(aq)}$), where the Henry's constant (K_H) for CO_2 in water at 25°C is approximately 3.4 x 10^{-2} (m/atm), two-step dissociation reactions, and the conservation of the total dissolved inorganic carbon (DIC) and total alkalinity (TA), ultimately determining pH and the distribution of carbonate species. The H_2CO_3 has two hydrogen ions and dissociates in two steps:

$$H_2CO_3 \overset{K_{a1}}{\longleftrightarrow} H^+ + HCO_3^- \qquad K_{a1} = 4.4\times10^{-7} \qquad \textbf{(4, in manuscript)}$$

$$HCO_3^- \overset{K_{a2}}{\longleftrightarrow} H^+ + CO_3^{2-} \qquad K_{a2} = 4.7\times10^{-11} \qquad \textbf{(5, in manuscript)}$$

The DIC can be expressed as

$$DIC = [H_2CO_3] + [HCO_3^-] + [CO_3^{2-}]$$
$$= K_H pCO_2^w + \frac{K_{a1} K_H pCO_2^w}{[H^+]} + \frac{K_{a1} K_{a2} K_H pCO_2^w}{[H^+]^2}$$
$$= K_H pCO_2^w \left(1 + \frac{K_{a1}}{[H^+]} + \frac{K_{a1} K_{a2}}{[H^+]^2}\right)$$
$$= K_H pCO_2^w([H^+]^2 + K_{a1}[H^+] + K_{a1} K_{a2})/[H^+]^2 \quad \text{(6, in manuscript)}$$

The marine carbonate system describes the distribution of DIC among its chemical species in seawater and is jointly governed by TA and pH. From Eq. (6), if the oceanic pCO_2^w and pH are known, the DIC can be determined, conversely, pCO_2^w can be inferred from DIC. TA is defined as the sum of the proton-neutralizing capacities of all weak acid anions in seawater (Dickson, 1981) and can be expressed as:

$TA=[HCO_3^-]+2[CO_3^{2-}]+[B(OH)_4^-]+[OH^-]+[HPO_4^{2-}]+2[PO_4^{3-}]+[SiO(OH)_3]+[NH_3]+[HS^-]-[H^+]-[H_3PO_4]$. In the POP2-waves framework, TA, pH and biogeochemistry are also used to calculate pCO_2^w.

When TA increases, the seawater becomes more alkaline, leading to an increase in CO_3^{2-} concentration and enhanced buffering of hydrogen ions. As a result, the $[H^+]$ decreases, causing pH to rise and increasing the ocean's capacity to absorb CO_2. Conversely, when TA decreases, the buffering capacity weakens, $[H^+]$ increases, pH decreases, and the ocean becomes more acidic with a reduced ability to uptake CO_2.

The biogeochemical module of POP2 (MARBL) updates TA in each grid cell by solving a coupled transport–reaction equation (Long et al., 2021). The average pH of the ocean is currently around 8.1 (Fig. 8c), reflecting slightly alkaline conditions. Within the DIC system, bicarbonate ions (HCO_3^-) are the dominant species because the prevailing pH lies between pK_{a1} and pK_{a2}. However, continued uptake of atmospheric CO_2 drives a decline in pH, a process termed ocean acidification. Our study highlights that wave-induced $K_{w,660}$ significantly influences the marine CO_2 system, altering alkalinity, pH, and carbonate speciation. These chemical changes, in turn, provide a feedback mechanism that modulates the overall dynamics of the air–sea CO_2 flux. In other words, perturbations in $K_{w,660}$ influence both $dpCO_2$ and air–sea CO_2 flux in the Earth System Model. This POP2–waves coupled behavior differs from traditional

approaches that treat wave-induced $K_{w,660}$ and $dpCO_2$ as independent variables when estimating air–sea CO_2 flux (e.g., Reichl and Deike, 2020).

Reference

Long, M. C., Moore, J. K., Lindsay, K., Levy, M., Doney, S. C., Luo, J. Krumhardt, K. M., Letscher, R. T., Grover, M., and Sylvester, T.: Simulations with the marine biogeochemistry library (MARBL). J. Adv. Model. Earth Sy., 13(12), e2021MS002647. https://doi.org/10.1029/2021MS002647, 2021.

RC2.15. Discussion: There is nontrivial overlap between the discussion and the results. Consider rewording so the results are explained alongside the figures, while the discussion puts these results in a broader context.

Response:

We have eliminated redundant content throughout the manuscript; consequently, the results are presented alongside the relevant figures and discussed within a broader scientific context.

RC2.16. L343: The differences between simulations don't suggest mitigation or enhancement (which is a separate mechanism), just different mean states. Please reword.

Response:

The differences in pH between POP2–waves and B–CTL are not simply due to different mean states. Rustogi et al. (2025) indicate that faster equilibration of oceanic pCO_2 in the wind–wave–bubble simulation, driven by enhanced gas exchange, reduces the air–sea partial pressure difference. This pCO_2 feedback is strongest in the extratropics, where it suppresses CO_2 uptake. Our POP2–waves experiment shows a similar response, with increasing pCO_2 (Fig. 8b) and hydrogen ion concentration, accompanied by decreasing pH (Fig. 8d) in the extratropics. Because atmospheric CO_2 is fixed at 367 ppm in the B_2000_CAM5 compsets, the reduced $dpCO_2$ suppresses negative air–sea CO_2 flux referred to as negative feedback from $dpCO_2$. Rustogi et al. (2025) also showed that the effects of $\Delta K_{w,660}$ (between wave-induced and based on U_{10}) and $\Delta dpCO_2$ partially offset each other, although the $\Delta K_{w,660}$ effect is generally 20%–30% stronger than the counteracting $\Delta dpCO_2$ effect, explaining the modest increase in both positive and negative air–sea CO_2 fluxes in the wind–wave–bubble simulation.

Reference

Rustogi, P., Resplandy, L., Liao, E., Reichl, B. G., and Deike, L.: Influence of wave-induced variability on ocean carbon uptake. Global Biogeochem. Cy., 39, e2024GB008382. https://doi.org/10.1029/2024GB008382, 2025.

RC2.17. Section 4.3/Figure 10: The point about the negative feedback from pCO_2 is not explored enough - how was this feedback shut off in the simulations? Note that Rustogi et al. (2025) go into this in detail. This is a key difference between models and observation-based products.

Response:

Rustogi et al. (2025) show that although wave-enhanced $K_{w,660}$ increases local air–sea CO_2 exchange, the resulting rise in oceanic pCO_2 reduces the air–sea pCO_2 gradient in the extratropics, generating a carbonate chemistry feedback that partially offsets the increase in global ocean carbon storage. Furthermore, Rustogi et al. (2025) note that because observation-based products do not account for pCO_2 feedback, they may yield larger departures in global carbon sink estimates when accounting for wave-driven processes.

Section 4.3 and Fig. 10 fully present the large deviations in the global ocean carbon sink estimates caused by the absence of pCO_2 feedback when wave effects are considered. The manuscript Eq. 1 shows that air–sea CO_2 flux is determined by both $K_{w,660}$ and $dpCO_2$. In the B_2000_CAM5 compset, atmospheric CO_2 concentration is fixed at the year-2000 mean value (367 ppm), meaning that oceanic pCO_2 does not feedback to atmospheric CO_2 concentration or modify near-surface atmospheric and oceanic conditions. Therefore, POP2–waves and B–CTL share the same surface wind, temperature, and related physical forcing fields. Section 4.3 is thus designed as a virtual experiment. We did not recalculate the full set of biogeochemical variables in order to isolate the influence of carbon flux calculations between POP2–waves and B–CTL. Instead, we combined the air–sea $dpCO_2$ values from B–CTL with the wave-enhanced $K_{w,660}$ from POP2–waves, rather than explicitly calculating a fully coupled virtual air–sea CO_2 flux. This experimental design applies wave-induced $K_{w,660}$ without the accompanying $dpCO_2$-driven negative feedback, thereby introducing substantial uncertainty into the estimated air–sea CO_2 flux.

$$FCO_2 = K_{w,660} \cdot k_0 \cdot (pCO_2^w - pCO_2^a) \cdot (1 - ice) \qquad \textbf{(1, in manuscript)}$$

Yes, pCO_2-driven negative feedback is a key difference between coupled models and observation-based products. Rustogi et al. (2025) highlighted that observation-based estimates, do not include pCO_2 feedback, which could potentially lead to larger deviations in global ocean carbon sink estimates when wave effects are considered.

Rustogi et al. (2025) demonstrate that while wave-enhanced *$K_{w,660}$* accelerates local air–sea CO_2 exchange, it simultaneously reduces the air–sea $dpCO_2$. However, the magnitude of the air–sea CO_2 flux overestimation resulting from the lack of this $dpCO_2$-driven negative feedback has not been fully quantified in recent studies. The "lack of $dpCO_2$-driven negative feedback" case, which does not include real ocean buffering effects, allows positive air–sea CO_2 flux regions to release excess CO_2 into the atmosphere (> 0.4 mol m^{-2} yr^{-1}) while simultaneously enhancing excess CO_2 uptake (< −0.4 mol m^{-2} yr^{-1}) in negative air–sea CO_2 flux regions (Fig. 10b) compared to the coupled POP2–waves model.

Other points:

RC2.18. L9: Consider rewording this line — "Wave and bubble mechanisms impact the air-sea CO_2 flux by enhancing the gas transfer velocity (kw), often modeled through significant wave height (Hs)".

Response:

Thank you for your comment. We have reworded the sentence as follows: "Wave and bubble processes influence air–sea CO_2 flux by enhancing the gas transfer velocity (K_w), which is commonly parameterized as a function of significant wave height (H_s). Please see revised manuscript for the change."

RC2.19. L85: I agree with the other reviewer that if the point about data assimilation is to be included, it should be better motivated.

Response:

Thank you for your comment. We removed the description of a single data assimilation method for reconstructing air–sea CO_2 flux validation data in L87 and replaced it with the following statement: most validation datasets are derived from sparse ship-based pCO_2 observations combined with statistical interpolation, machine learning, atmospheric inversion, and climatological

averaging to construct gridded long-term flux products. Please see revised manuscript for the change.

RC2.20. L92: Are you thinking of observation-based products when you reference non-model simulations? Please reword for clarity.

Response:

Yes, we refer to surface ocean observation-based products. Please see the revised manuscript for these changes.

RC2.21. Spell out acronyms WP and EP.

Response:

WP denotes the Western Pacific region (160–180°E, 35–40°N), and EP denotes the Equatorial Pacific region (230–250°E, 0–5°S). Please see the revised manuscript for these changes.